Acta Crystallographica Section D
Biological Crystallography
ISSN 0907-4449

Structure of the G225P/G226P mutant of mouse 3(17)α-hydroxysteroid dehydrogenase (AKR1C21) ternary complex: implications for the binding of inhibitor and substrate

Urmi Dhagat,[a]‡ Satoshi Endo,[b]‡ Hiroaki Mamiya,[b] Akira Hara[b] and Ossama El-Kabbani[a]*

[a]Medicinal Chemistry and Drug Action, Monash Institute of Pharmaceutical Sciences, Monash University, Parkville, Victoria 3052, Australia, and [b]Laboratory of Biochemistry, Gifu Pharmaceutical University, Mitahora-higashi, Gifu 502-8585, Japan

‡ These authors contributed equally to this work.

Correspondence e-mail: ossama.el-kabbani@vcp.monash.edu.au

Received 1 November 2008
Accepted 26 December 2008

PDB Reference:
G225P/G226P mutant 3(17)α-hydroxysteroid dehydrogenase–NADP$^+$–hexoestrol complex, 3cv6, r3cv6sf.

3(17)α-Hydroxysteroid dehydrogenase (AKR1C21) is a unique member of the aldo-keto reductase (AKR) superfamily owing to its ability to reduce 17-ketosteroids to 17α-hydroxysteroids, as opposed to other members of the AKR family, which can only produce 17β-hydroxysteroids. In this paper, the crystal structure of a double mutant (G225P/G226P) of AKR1C21 in complex with the coenzyme NADP$^+$ and the inhibitor hexoestrol refined at 2.1 Å resolution is presented. Kinetic analysis and molecular-modelling studies of 17α- and 17β-hydroxysteroid substrates in the active site of AKR1C21 suggested that Gly225 and Gly226 play an important role in determining the substrate stereospecificity of the enzyme. Additionally, the G225P/G226P mutation of the enzyme reduced the affinity (K_m) for both 3α- and 17α-hydroxysteroid substrates by up to 160-fold, indicating that these residues are critical for the binding of substrates.

1. Introduction

Hydroxysteroid dehydrogenases are divided into two different protein superfamilies: the short-chain dehydrogenases/reductases (Oppermann *et al.*, 2003) and the aldo-keto reductases (AKRs; Jez & Penning, 2001). Members of the AKR superfamily are monomeric NADPH-dependent enzymes that possess a triose phosphate isomerase (TIM) barrel motif consisting of an eight-stranded parallel β-sheet at the core surrounded by eight α-helices (Jez *et al.*, 1997). Based on the types of reactions catalysed by these enzymes, they are further classified into subfamilies. Of particular interest is the AKR1C subfamily, which comprises enzymes that are involved in the activation/inactivation of steroid hormones through their oxidoreductase activities (Penning *et al.*, 1997). The members of this subfamily are important drug targets owing to their role in regulating the amount of steroid hormone that can bind to and activate receptors (Penning, 2003).

NADP$^+$-dependent 3(17)α-hydroxysteroid dehydrogenase (EC 1.1.1.209) was first purified from the liver and kidneys of rabbits (Lau *et al.*, 1982*a*,*b*) and mice (Nakagawa *et al.*, 1989). The cDNA for the mouse enzyme has been cloned (Ishikura *et al.*, 2004; Bellemare *et al.*, 2005) and is currently annotated as the 21st member of the AKR1C subfamily (AKR1C21). Like other members of the AKR1C subfamily, AKR1C21 can act as either a hydroxysteroid dehydrogenase or a ketosteroid reductase depending on the cellular NADP$^+$:NADPH ratio (Penning *et al.*, 2000). An outstanding feature of AKR1C21 is its bifunctional activity, which reduces/oxidizes the keto/hydroxyl groups at positions 3 and 17 of steroid substrates but

to varying extents (Ishikura *et al.*, 2004). AKR1C21 catalyses the reduction of 21-hydroxy-5α-pregnane-3,20-dione and 5α-pregnane-3,20-dione into the corresponding 3α-hydroxysteroids, which are potent positive modulators of the γ-aminobutyric acid type A receptor (Rupprecht & Holsboer, 1999; Morris *et al.*, 1999). The 17α-hydroxysteroid dehydrogenase activity of the enzyme is unique; other members of the AKR1C subfamily exhibit 17β-hydroxysteroid dehydrogenase activity (Penning *et al.*, 2000; Matsunaga *et al.*, 2006). The reduction of 4-androstene-3,17-dione by the enzyme yields epitestosterone (epi-T), a 17α-epimer of testosterone (TES), which has been linked to the development of breast and prostate cancers (Bellemare *et al.*, 2005). Characterization of the interactions between the inhibitor hexoestrol and the active-site residues may lead to the design of new compounds that can inhibit the 17α-reductase activity of AKR1C21 that is associated with cancer development.

In our attempts to identify the structural determinants for the bifunctional activity of AKR1C21, the crystal structure of the binary complex with NADPH bound was determined and probed using molecular-modelling studies of steroid substrates (Dhagat *et al.*, 2007). The models showed that the 17-ketosteroid and 3α-hydroxysteroid (or 3-ketosteroid) substrates were oriented differently in the active site and hence were involved in hydrogen-bonding interactions with different residues lining the substrate-binding cavity. The key determinants of substrate recognition as well as product release were suggested to be the amino-acid residues Lys31 for the 17α-hydroxysteroid dehydrogenase activity and Gly225 and Gly226 for the 3α-hydroxysteroid dehydrogenase activity. The role of Lys31 has been supported by crystallographic and mutagenesis studies, which show its importance for substrate stability during catalysis (Faucher *et al.*, 2007). However, the proposed roles of Gly225 and Gly226 have not been validated by other analyses and there is currently no report on the involvement of the residues at positions 225 and 226 in substrate recognition by enzymes of the AKR superfamily, apart from the suggestion that Thr226 of rat 3α-hydroxysteroid dehydrogenase (AKR1C9) is implicated in substrate binding (Bennett *et al.*, 1997).

AKR1C21 is inhibited by synthetic oestrogens, 17β-oestradiol and several aldose-reductase inhibitors (Ishikura *et al.*, 2004; Dhagat *et al.*, 2008). Our molecular-modelling and kinetic studies showed that aldose-reductase inhibitors display competitive and noncompetitive inhibition with respect to the substrate and possess a core template that is held in place by hydrogen bonding and van der Waals interactions and a polar head that interacts with the catalytic residues His117 and Tyr55 of AKR1C21 (Dhagat *et al.*, 2008). Knowledge of the residues involved in substrate and inhibitor binding may be useful in the design of potent and selective AKR1C21 inhibitors, which is important owing to the pivotal role of the enzyme in the intracrine regulation of hormonal steroids.

In this study, using site-directed mutagenesis, we replaced Gly225 and Gly226 of AKR1C21 with proline residues (G225P/G226P), which are rigid and cannot form hydrogen bonds. The mutant enzyme (MT-C21) was purified and the kinetic constants for hydroxysteroids were compared with those of the wild-type enzyme (WT-C21). Surprisingly, MT-C21 displayed 17β-hydroxysteroid dehydrogenase activity towards TES and 5α-androstan-17β-ol-3-one (5α,17β-AND), as well as significant decreases in catalytic activity towards 5α-pregnane-3α,20α-diol (5α-PREG) and epi-T. In addition, we determined the first crystal structure of MT-C21 in complex with $NADP^+$ and the synthetic oestrogen inhibitor hexoestrol and investigated the roles of Gly225 and Gly226 in inhibitor binding and substrate stereoselectivity by molecular modelling.

2. Materials and methods

2.1. Site-directed mutagenesis and purification of recombinant enzymes

Mutagenesis of G225P/G226P was performed using a QuikChange site-directed mutagenesis kit (Stratagene) and a pkk223-3 expression plasmid harbouring cDNA encoding the entire 323-amino-acid sequence of AKR1C21 as the template according to the protocol described by the manufacturer (Ishikura *et al.*, 2004). The 40-mer primer pair used for mutagenesis was composed of sense and antisense oligonucleotides to alter the codons (GGA) for Gly225 and Gly226 of AKR1C21 cDNA to the codon (CCA) for proline. The coding region of the cDNA in the expression plasmid was sequenced using a Beckman CEQ2000XL DNA sequencer in order to confirm the presence of the desired mutation and to ensure that no other mutations had occurred. The recombinant WT-C21 and MT-C21 enzymes were expressed in *Escherichia coli* JM109 and purified to homogeneity as described previously (Ishikura *et al.*, 2004). Purity was confirmed by SDS–PAGE and protein concentration was determined using a bicinchoninic acid protein-assay reagent kit (Pierce, Rockford, Illinois, USA) using bovine serum albumin as the standard.

2.2. Crystallization

The MT-C21 ternary complex was crystallized using the hanging-drop vapour-diffusion method and the published conditions for the WT-C21 binary complex (El-Kabbani *et al.*, 2005). Crystals were obtained from 0.1 *M* HEPES pH 7.5, 10% polyethylene glycol 6000, 5% 2-methyl-2,4-pentanediol. hexoestrol (Sigma–Aldrich) was dissolved in methanol, with the final concentration of methanol not exceeding 2% of the total volume of the ternary complex. $NADP^+$ and hexoestrol were added to MT-C21 in a molar ratio of 1:3:3. The final concentration of the protein in the ternary complex was 18 mg ml^{-1} and droplets were prepared by mixing 3 µl of the ternary complex with an equal volume of crystallization buffer. The mixture was placed on siliconized cover slips and allowed to equilibrate against 1 ml reservoir solution at 295 K.

2.3. Data collection and analysis

The crystals used for X-ray diffraction analysis were soaked in a cryoprotective solution (20% ethylene glycol added to the mother liquor) and flash-cooled at 100 K. Diffraction data

were collected on a MAR345 image-plate system mounted on a Rigaku RU300 rotating-anode generator operating at 50 kV and 90 mA and were processed using *HKL*-2000 and *SCALEPACK* (Otwinowski & Minor, 1997). The structure was solved by molecular replacement using the program *MOLREP* from the *CCP*4 suite of crystallographic software (Collaborative Computational Project, Number 4, 1994; Storoni *et al.*, 2004), with the atomic coordinates of WT-C21 (PDB code 2p5n; Dhagat *et al.*, 2007) as the search model. Following an initial round of rigid-body refinement, the structure was subjected to several rounds of noncrystallographic symmetry-restrained refinement and manual fitting of the amino-acid side chains into $2F_o - F_c$ and $F_o - F_c$ electron-density maps. The refinement procedure was performed using *REFMAC*5 and the difference Fourier maps ($2F_o - F_c$ and $F_o - F_c$) were visualized in *Coot* (Murshudov *et al.*, 1997; Emsley & Cowtan, 2004). In the final stages of the refinement, the cofactor, inhibitor and water molecules were added to the model. The structure was validated using *PROCHECK* (Laskowski *et al.*, 1993). A summary of the data-collection and refinement statistics is presented in Table 1.

Table 1
Summary of data-collection and refinement statistics.

Values in parentheses are for the highest resolution shell.

Data collection and processing	
X-ray source	Rigaku RU300
Detector	MAR scanner 345 mm plate
Wavelength (Å)	1.54179
Unit-cell parameters (Å, °)	$a = b = 102.10$, $c = 72.27$, $\alpha = \beta = 90$, $\gamma = 120.0$
Space group	$P3_2$
Diffraction data	
Resolution range (Å)	30–2.1 (2.18–2.1)
Total no. of reflections	186830 (19484)
Unique reflections	46635 (4802)
Completeness (%)	99.8 (100)
Redundancy	4.0 (4.4)
$I/\sigma(I)$	16.7 (2.2)
R_{merge}† (%)	3.9 (36.7)
Refinement (30–2.1 Å)	
R_{free}‡	0.256
R_{work}‡	0.197
Protein residues (dimer)	646
$NADP^+$ molecules	2
BME molecules	2
Hexoestrol molecules	2
Water molecules	664
R.m.s. deviations	
Bonds (Å)	0.016
Angles (°)	1.7
Ramachandran plot	
Residues in favoured regions (%)	90.9
Residues in allowed regions (%)	8.7
Residues in disallowed regions (%)	0.4
Estimated coordinate error	
Luzzati plot (Å)	0.262
Average B factors (Å^2)	
Protein (chains A + B)	36.4
$NADP^+$	32.2
BME	57.8
Hexoestrol	55.2
Waters	40.0

† $R_{merge} = \sum_{hkl}\sum_i |I_i(hkl) - \langle I(hkl)\rangle| / \sum_{hkl}\sum_i I_i(hkl)$, where $\langle I(hkl)\rangle$ is the average intensity over symmetry-related reflections and $I_i(hkl)$ is the observed intensity. ‡ R value $= \sum ||F_o| - |F_c|| / |F_o|$, where F_o and F_c are the observed and calculated structure factors. For R_{free} the sum is performed on the test-set reflections (5% of total reflections) and for R_{work} it is performed on the remaining reflections.

2.4. Assay of enzyme activity

The dehydrogenase and reductase activities were assayed by measuring the rate of change of NADPH fluorescence (at 455 nm, using an excitation wavelength of 340 nm) and absorbance (at 340 nm), respectively, at 298 K. The reaction mixture for the dehydrogenase activity consisted of 0.1 *M* potassium phosphate buffer pH 7.0, 0.25 m*M* $NADP^+$, hydroxysteroid and enzyme in a total volume of 2.0 ml. NADPH (0.1 m*M*) was used as the coenzyme in the assay of the reductase activity for ketosteroids. The rate was corrected for the non-enzymatic increase in fluorescence at 455 nm or the decrease of absorbance at 340 nm in the mixture without enzyme or substrate. The IC_{50} value (the inhibitor concentration required for 50% inhibition) for hexoestrol was determined in the presence of saturating concentrations of epi-T (5 µ*M* for WT-C21 and 50 µ*M* for MT-C21). The apparent K_m and k_{cat} values for substrates were determined by fitting the initial velocities to the Michaelis–Menten equation. The kinetic constants and IC_{50} values are expressed as the means ± standard deviations of at least three determinations. Steroids were obtained from Steraloids (Newport, Rhode Island, USA) and Sigma–Aldrich Chemicals.

2.5. Product identification

To identify the reaction products, reduction was conducted in a 2.0 ml system containing 0.2 m*M* NADPH, 50 µ*M* substrate, 10 µg enzyme and 0.1 *M* potassium phosphate pH 7.4. The substrate and products were extracted into 4 ml ethyl acetate 30 min after the reaction was started at 310 K and were analysed by thin-layer chromatography (TLC) using silica-gel-coated plates. The TLC chromatogram was developed in chloroform/ethyl ether [9:1(*v*:*v*)] four times and the products and cochromatographed authentic steroids were visualized by spraying with ethanol/H_2SO_4 [1:1(*v*:*v*)] solution and heating at 383 K for 1 h.

2.6. Molecular docking and energy minimization

3-Hydroxysteroid and 17-hydroxysteroid substrates were manually docked with their 3-hydroxyl and 17-hydroxyl groups, respectively, pointing towards the coenzyme and the catalytic residues of WT-C21 and MT-C21 following previously published criteria for optimal steroidal substrate positioning inside the active-site pocket (Bennett *et al.*, 1997; Couture *et al.*, 2003; Nahoum *et al.*, 2001). The torsion angles of the residues lining the substrate-binding cavity, such as Trp227 and Leu27, were manually adjusted in order to avoid short contacts with the docked substrates. H atoms, partial charges, atomic potentials and bond orders were assigned to the enzyme–substrate complexes using the automatic procedures within the *InsightII* 2.1 package (Biosym Technologies Inc., San Diego, California, USA). $NADP^+$ was used as the coenzyme for the oxidation of hydroxysteroids. The

complexes with active substrates were energy-minimized to eliminate steric hindrance between the substrates and the amino-acid residues of the active site using the *Discover* 2.7 package (Biosym Technologies Inc., San Diego, California, USA) on a Linux workstation following published protocols found to be effective for visualizing a protein–ligand complex in its lowest energy conformation (Darmanin & El-Kabbani, 2000, 2001). Figures were generated using *PyMOL* (DeLano Scientific, San Carlos, California, USA).

3. Results

3.1. Alteration of kinetic constants and steroid specificity by the mutation

The kinetic effect of the mutation was assessed by comparing the kinetic constants for the forward (Table 2) and reverse (Table 3) direction of the reaction for WT-C21 and MT-C21. In the forward reaction, the most striking alteration caused by the G225P/G226P mutation was the increase in the K_m value for the 3α-hydroxysteroid 5α-PREG, which is contrary to the alteration in the value observed for 5β-pregnane-3α,20α-diol (5β-PREG). In the oxidation of 17α-hydroxysteroids, the mutation resulted in moderate increases in the K_m values for epi-T and 5α-androstan-17α-ol-3-one (5α,17α-AND) and a small effect on the K_m value for 5β-androstan-17α-ol-3-one (5β,17α-AND). Interestingly, the mutant enzyme exhibited dehydrogenase activity towards TES and 5α,17β-AND that was not observed with WT-C21. It should be noted that dehydrogenase activity of MT-C21 was not observed for 3β-hydroxysteroids (5α/β-androstan-3β-ol-17-ones and 5α/β-pregnane-3β,20α-diols) and 20-hydroxysteroids (5α/β-pregnan-20α-ol-3-ones). In the reverse reaction, MT-C21 reduced both 4-androstene-3,17-dione and 5α-androstan-3α-ol-17-one (5α,3α-AND) with higher K_m values compared with WT-C21 (Table 3) and produced the 17α- and 17β-hydroxymetabolites of the two ketosteroids, in contrast to the formation of only their 17α-hydroxy metabolites by WT-C21 (Fig. 1). Thus, the double G225P/G226P mutation converted AKR1C21 into an enzyme form that shows high selectivity for 5β-PREG in the oxidation of the 3α-hydroxy group and, conversely, broad specificity for both 17α- and 17β-hydroxysteroids.

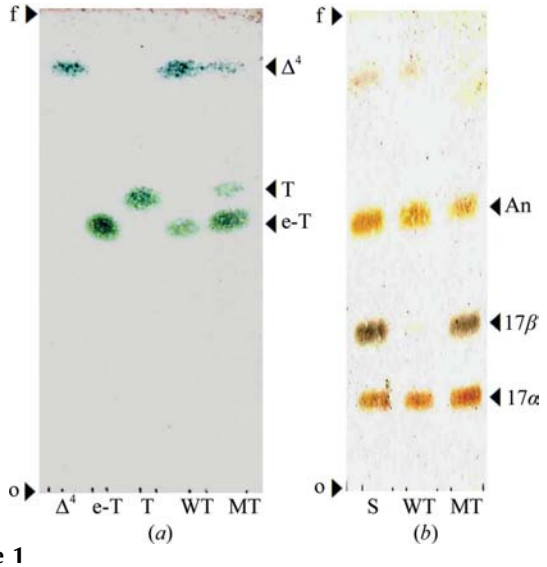

Figure 1
Product identification by TLC in the reduction of 17-ketosteroids by WT-C21 and MT-C21. (*a*) Authentic samples: 4-androstene-3,17-dione (Δ^4), epi-T (e-T) and TES (T). The samples were developed from the origin (o) to the front (f) on the silica-gel plate. WT-C21 (WT) produced only the 17α-hydroxy metabolite e-T, whereas MT-C21 (MT) yielded both e-T and the 17β-hydroxy metabolite T. (*b*) Authentic samples (S) include 5α,3α-AND (An), 5α-androstane-3α,17β-diol (17β) and 5α-androstane-3α,17α-diol (17α). WT-C21 produced only 17α, whereas MT-C21 yielded both 17α and 17β.

Table 2
Kinetic alteration in the oxidation of hydroxysteroids by the G225P/G226P mutation.

Substrate (abbreviation)	WT-C21†	MT-C21	Ratio‡
5α-Pregnane-3α,20α-diol (5α-PREG)			
K_m (μM)	0.5	80 ± 10	160
k_{cat} (min^{-1})	6.3	9.0 ± 1.0	1.4
k_{cat}/K_m (min^{-1} μM^{-1})	13	0.1	0.008
5β-Pregnane-3α,20α-diol (5β-PREG)			
K_m (μM)	0.6	2.9 ± 0.3	5
k_{cat} (min^{-1})	13	11 ± 1	0.8
k_{cat}/K_m (min^{-1} μM^{-1})	22	3.8	0.2
Epitestosterone (epi-T)			
K_m (μM)	0.6	18 ± 1	30
k_{cat} (min^{-1})	18	15 ± 1	0.8
k_{cat}/K_m (min^{-1} μM^{-1})	30	0.8	0.02
5α-Androstan-17α-ol-3-one (5α,17α-AND)			
K_m (μM)	0.4	4.8 ± 0.9	12
k_{cat} (min^{-1})	10	8.7 ± 0.6	0.9
k_{cat}/K_m (min^{-1} μM^{-1})	25	1.8	0.07
5β-Androstan-17α-ol-3-one (5β,17α-AND)			
K_m (μM)	0.4	1.3 ± 0.1	3
k_{cat} (min^{-1})	8.4	3.3 ± 0.3	0.4
k_{cat}/K_m (min^{-1} μM^{-1})	21	2.5	0.1
Testosterone (TES)			
K_m (μM)		23 ± 1	—
k_{cat} (min^{-1})	na§	2.4 ± 0.1	—
k_{cat}/K_m (min^{-1} μM^{-1})		0.1	—
5α-Androstan-17β-ol-3-one (5α,17β-AND)			
K_m (μM)		27 ± 2	—
k_{cat} (min^{-1})	na§	23 ± 2	—
k_{cat}/K_m (min^{-1} μM^{-1})		0.85	—

† The values for WT-C21 are taken from Ishikura *et al.* (2004). ‡ Ratio of the value for MT-C21 to that for WT-C21. § na, no activity was detected with 50 μM steroid.

3.2. Structure of the ternary complex

Following extensive cocrystallization trials, crystals of MT-C21 in a ternary complex with the coenzyme $NADP^+$ and the inhibitor hexoestrol were successfully grown. The structure of the complex was determined in space group $P3_2$ at a resolution of 2.1 Å. There were two monomers in the asymmetric unit, with a calculated solvent content of 51% and a Matthews coefficient of 2.54 $Å^3$ Da^{-1}. In the refined crystal structure there were 646 amino-acid residues (each monomer consists of 323 amino-acid residues), two hexoestrol, two $NADP^+$, five β-mercaptoethanol (BME) and 664 water molecules. The backbone dihedral angles of 90.9% of the residues were in the most favoured regions and those of 8.7% were in additionally allowed regions of the Ramachandran plot. Only Thr221 was in the disallowed region of the Ramachandran plot owing to

Table 3
Kinetic alteration in the reduction of 17-ketosteroids by the G225P/G226P mutation.

Substrate	WT-C21†	MT-C21	Ratio‡
4-Androstene-3,17-dione			
K_m (μM)	0.2	0.9 ± 0.1	4.5
k_{cat} (min^{-1})	10	8.2 ± 0.2	0.8
k_{cat}/K_m (min^{-1} μM^{-1})	50	9	0.2
5α-Androstan-3α-ol-17-one			
K_m (μM)	0.6 ± 0.1	9.7 ± 1.4	16
k_{cat} (min^{-1})	4.4 ± 0.3	13 ± 0.5	3
k_{cat}/K_m (min^{-1} μM^{-1})	7.3	1.3	0.2

† The values without standard errors for WT-C21 are taken from Ishikura *et al.* (2004). ‡ Ratio of the value for MT-C21 to that for WT-C21.

the hydrogen bond present between the main chain and the cofactor. The crystal structure of the WT-C21 binary complex was determined at 1.8 Å resolution from an orthorhombic crystal belonging to space group $P2_12_12_1$ (Dhagat *et al.*, 2007). The estimated coordinate errors for MT-C21 and WT-C21 were 0.262 and 0.248 Å, respectively. The overall fold of MT-C21 is similar to that of WT-C21, apart from the loop region lining the active-site pocket, in which the two glycines at positions 225 and 226 were mutated to prolines which have a more rigid structure, resulting in a larger substrate-binding pocket. This is depicted in Fig. 2(*a*), in which the crystal structures of MT-C21 and WT-C21 are superimposed. A comparison of the two crystal structures shows that the mutation affects the conformation of the adjoining residues Tyr224 and Trp227, resulting in a further opening up of the active-site pocket while the catalytic residues remain unaffected. The representative electron density for the two proline residues in MT-C21 is shown in Fig. 2(*b*). The inhibitor molecule is bound to the active site with one hydroxyl group pointing towards the catalytic residues, within hydrogen-bonding distance of His117 (2.8 Å) and Tyr118 (3.1 Å), while the other hydroxyl group hydrogen bonds to Lys31 (3.5 Å) and the main-chain atoms of Tyr55 (3.3 Å) and Leu25 (2.8 Å). The bulky phenyl rings and the methyl groups of hexoestrol form van der Waals contacts with Trp227, Tyr224, Tyr55 and the nicotinamide ring of $NADP^+$ (<4 Å). The chemical structure of hexoestrol and its interactions with the active-site residues of WT-C21 are shown in Figs. 3 and 4, respectively. Since Pro225 and Pro226 are not present within van der Waals contact of hexoestrol (>4 Å), the IC_{50} values of hexoestrol for WT-C21 and MT-C21 were 0.26 ± 0.02 and 0.60 ± 0.06 μM, respectively, confirming that the mutation had little effect on binding of the inhibitor.

3.3. Molecular modelling

In order to explain the alterations in kinetic constants and steroid specificity upon mutation, we studied the interactions of 3α-, 17α- and 17β-hydroxysteroid substrates with WT-C21 and MT-C21 by molecular modelling. The substrates were docked into the active sites of the crystal structures of the enzymes and the active complexes were energy-minimized to determine low-energy binding conformations as described in §2.6.

3.3.1. 3α-Hydroxysteroids. Energy-minimized models of WT-C21 and MT-C21 with 5α-PREG and 5β-PREG docked in

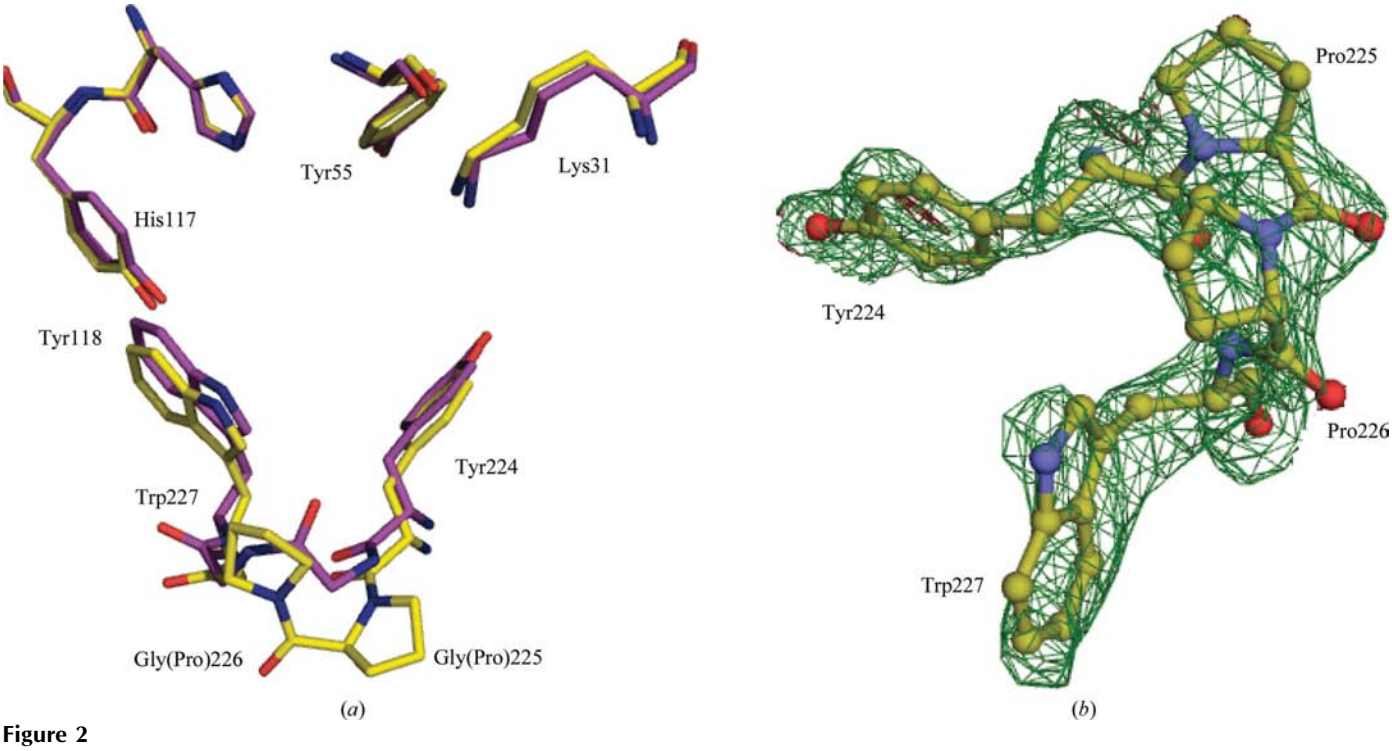

Figure 2
(*a*) Comparison of the steroid-binding site in WT-C21 and MT-C21. Superimposition of the residues lining the binding site of WT-C21 (pink) and MT-C21 (yellow) show how the mutation causes the active-site pocket to open up. (*b*) The final σ_A-weighted $F_o - F_c$ electron-density map, calculated at a 2.5σ cutoff after omitting the two prolines and adjoining residues (224–227), is shown in green.

their active sites are shown in Fig. 5. In WT-C21 and MT-C21 both substrates make similar interactions with the catalytic residues Tyr55 and His117. However, in WT-C21 5α-PREG forms hydrogen bonds to both Gly225 (2.6 Å) and Gly226 (3.0 Å), whereas 5β-PREG only forms a hydrogen bond to Gly226 (3.5 Å). This is a consequence of the different fusion of the A and B rings in 5α-PREG (*trans* union) and 5β-PREG (*cis* union) and the resulting effect on the binding of the steroid molecules. In case of 5β-PREG the 3-hydroxyl group is bent upwards, allowing it to sit deeper in the active-site pocket compared with 5α-PREG. As such, 5β-PREG is not within hydrogen-bonding distance of Gly225. In MT-C21 both substrates lose their hydrogen bonds to the glycines, which explains the increase in K_m values for the two substrates, with the larger effect being observed for 5α-PREG (Table 2).

3.3.2. 17α-Hydroxysteroids. Epi-T, 5α,17α-AND and 5β,17α-AND were docked and energy-minimized in both WT-C21 and MT-C21 (Fig. 6). The models suggest that the substrates are held in position by hydrogen bonds to Lys31 as well as to the catalytic residues His117 and Tyr55, which is consistent with the findings from previous studies that identified Lys31 as an important residue for substrate binding and catalysis of AKR1C21 (Faucher *et al.*, 2007; Dhagat *et al.*, 2007). The final conformation of epi-T in our model following energy minimization is similar to the published crystal structure of the AKR1C21–epi-T complex (Faucher *et al.*, 2007), which in turn validates our modelling approach (Fig. 6*c*). Nonetheless, following energy minimization of the MT-C21 complex, epi-T loses its hydrogen bond to Lys31. The replacement of glycines with prolines causes a shift in the positions of the adjoining residues Tyr224 and Trp227, which results in loose binding of the substrate in the active site owing to the loss of important van der Waals contacts with Trp227 and Tyr224. This explains the increase in K_m values for these

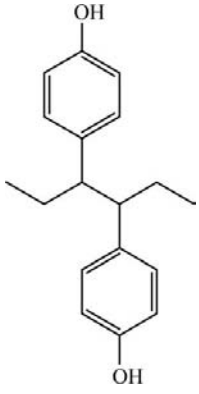

Figure 3
Chemical structure of hexoestrol.

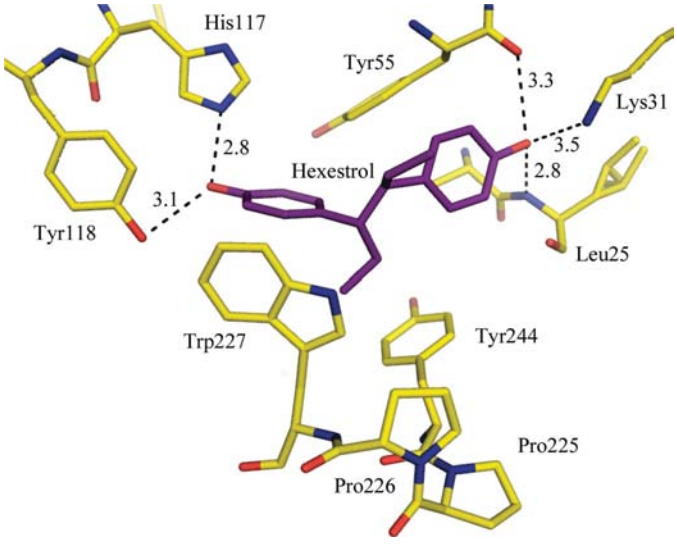

Figure 4
Hydrogen-bond interactions between the inhibitor hexoestrol (purple) and the active-site residues (yellow) of MT-C21 are shown as dashes and the respective distances are given in Å.

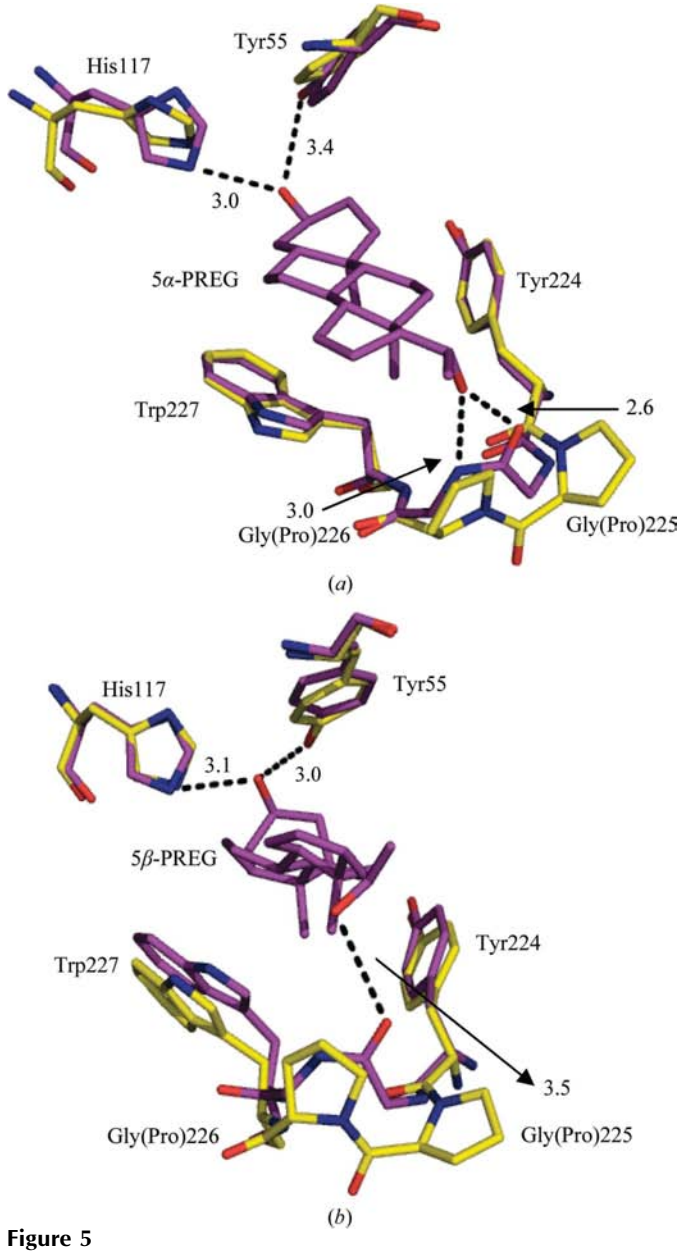

Figure 5
Energy-minimized crystal structures of WT-C21 (purple) and MT-C21 (yellow) with 5α-PREG (*a*) and 5β-PREG (*b*) modelled in the active sites.

substrates in MT-C21 despite the fact that they do not make direct contacts with the mutated residues.

3.3.3. 17β-Hydroxysteroids. Since 17β-hydroxysteroids were not catalysed by WT-C21, they were initially docked and energy-minimized in MT-C21 and then superimposed onto the crystal structure of WT-C21 for comparison (Fig. 7). Analysis of the models of 5α,17β-AND and TES suggests that both these substrates undergo catalysis by MT-C21 owing to the opening up of the active-site pocket as a result of the mutation, allowing access to the catalytic residues. In WT-C21 these substrates are unable to bind in the active site owing to steric hindrance resulting from residues lining the substrate-binding cavity as shown in Fig. 7, in particular the short contacts that occur with the side chain of Trp227 (<2 Å).

4. Discussion

Since AKR1C21 is the only enzyme known to stereospecifically oxidize 17α-hydroxysteroids, we have identified the determinants of the stereospecificity of this enzyme by investigating the residues lining the substrate-binding pocket. Kinetic analysis of WT-C21 and MT-C21 showed that the two glycines at positions 225 and 226 in the wild type allow tight binding of the substrates in the active site, contributing to the stereospecificity of the enzyme. Molecular-modelling analysis showed that various substrates are held in position *via* hydrogen bonds and van der Waals contacts with seven residues lining the active site (Lys31, Tyr55, His117, Tyr224, Gly225, Gly226 and Trp227) that play a direct role in determining the selectivity for substrates. In MT-C21 the inability of Pro225 and Pro226 to form hydrogen bonds to the substrates results in an increase in the K_m values and a consequential decrease in the k_{cat}/K_m values. This is clearly exemplified in the case of 5α-PREG, which forms hydrogen bonds to both Gly225 and Gly226 in WT-C21. The loss of the hydrogen bonds is accompanied by a 160-fold increase and 125-fold decrease in the K_m and k_{cat}/K_m values, respectively, in MT-C21.

3α-Hydroxysteroids are the only substrates that directly interact with Gly225 and Gly226 and as such they show the largest changes in catalytic activity upon mutation. 17α-Hydroxysteroids, which do not directly interact with the two glycines, also displayed an increase in K_m and a decrease

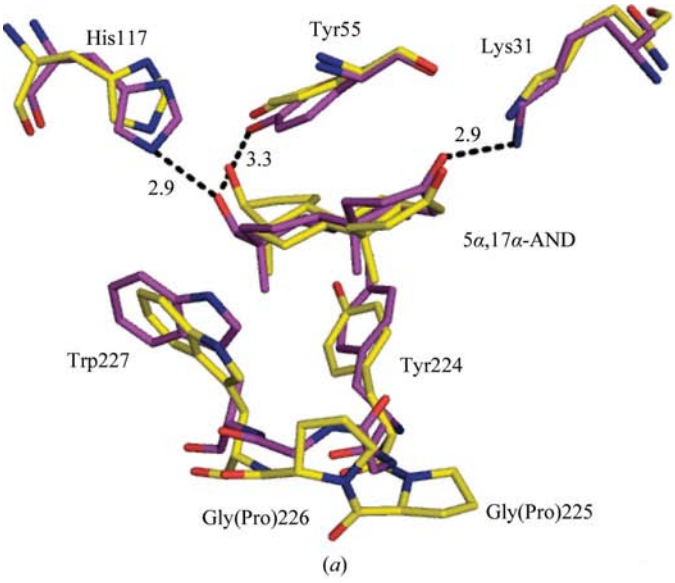

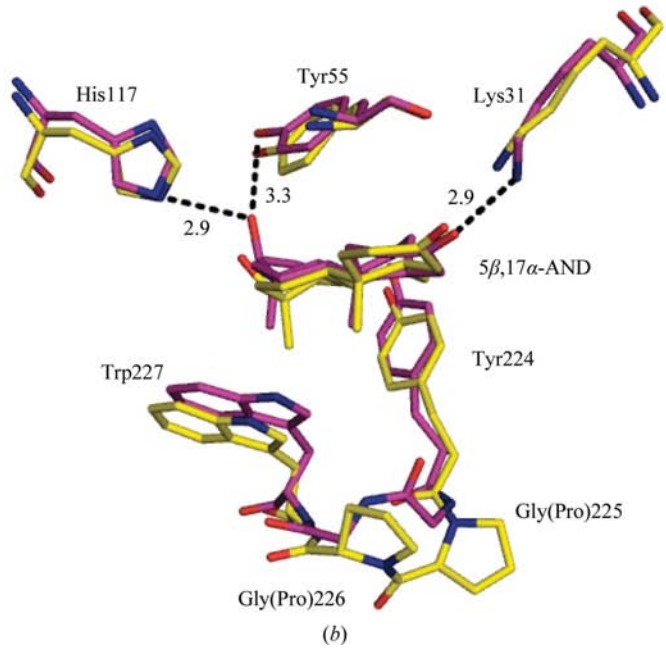

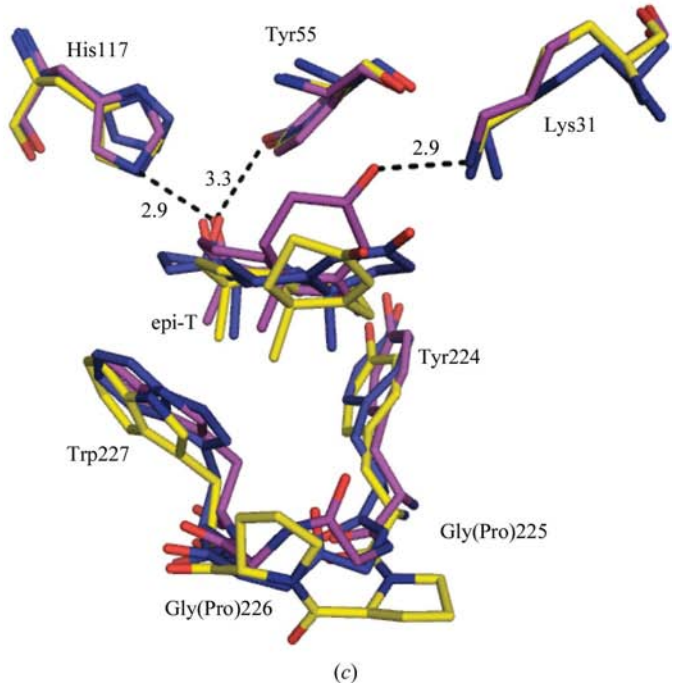

Figure 6
Energy-minimized crystal structures of WT-C21 (purple) and MT-C21 (yellow) with 5α,17α-AND (*a*) and 5β,17α-AND (*b*) modelled in the active sites. (*c*) Energy-minimized crystal structures of WT-C21 (purple) and MT-C21 (yellow) with epi-T modelled in the active sites superimposed on the crystal structure of WT-C21 (blue) with bound epi-T (Faucher *et al.*, 2007)

in k_{cat}/K_m values in MT-C21. Models of the docked 17α-hydroxysteroids show that their hydrogen bonds to the catalytic residues are almost unaffected by the mutation; however, the hydrogen-bond distance between the 17α-hydroxysteroids and Lys31 increases in MT-C21, suggesting that this part of the substrate molecule is not held tightly in the binding pocket. In the case of epi-T there is a complete loss of the hydrogen bond to Lys31, although this may not be entirely responsible for the observed reduction in the catalytic efficiency of the mutant. In MT-C21, the replacement of the two glycines with prolines results in an observed shift of the adjoining residues to accommodate the bulky proline rings and thus changes the overall shape of the active-site pocket. This makes the active-site pocket larger, thereby compromising the van der Waals contacts between these residues and the substrates, which is likely to contribute to the decrease in the affinity of the enzyme for the substrates.

The apparent activity of MT-C21 towards TES and 5α,17β-AND, which are not oxidized by WT-C21, suggests that the mutation also affects the stereospecificity of the enzyme. The fact that the substrates are not catalysed by WT-C21 suggests that they do not fit into the binding pocket, possibly owing to steric hindrance resulting from residues such as Trp227. Models of these substrates suggest that the active-site pocket of MT-C21, which is larger than that of the WT-C21, allows 17β-hydroxysteroids to bind with no steric hindrance resulting from the surrounding residues, thus explaining the appearance of 17β-hydroxysteroid dehydrogenase activity.

In summary, crystal structure determination complemented by kinetic analysis and molecular modelling of 17α- and 17β-hydroxysteroids in the active site of AKR1C21 suggests that Gly225 and Gly226 play an important role in determining the substrate stereospecificity of AKR1C21. The mutation of the two glycines reduces the affinity of the enzyme for both 3α- and 17α-hydroxysteroids, confirming that these residues are critical for maintaining the proper shape of the active-site pocket, allowing tight binding of the substrates. The first crystal structure of AKR1C21 in complex with a potent inhibitor, hexoestrol, is in agreement with inhibitor-binding studies suggesting that Gly225 and Gly225 may not play an important role in positioning the inhibitor in the active site. However, knowledge of the binding mode of hexoestrol and the residues (Leu25, Lys31, Tyr55, His117, Tyr118, Tyr224 and Trp227) involved in lining the inhibitor-binding site in AKR1C21 may be useful in the development of anticancer drugs through their 17α-reductase inhibitory activity.

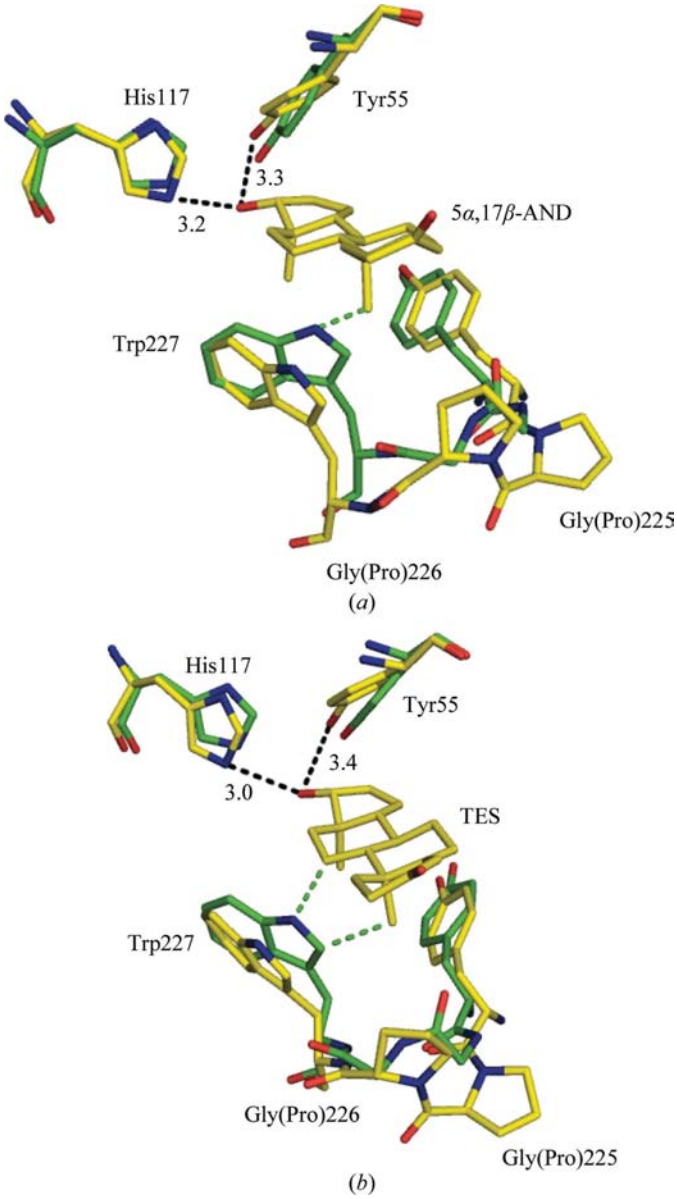

Figure 7
Energy-minimized crystal structures of MT-C21 with 5α,17β-AND (*a*) and TES (*b*) modelled in the active site are shown in yellow. The hydrogen bonds between the substrates and the mutant enzyme are labelled and shown as blue dashes. These models are superimposed on the unminimized crystal structure of WT-C21 (green) and the short contacts made by these substrates in WT-C21 are shown as green dashes.

References

Bellemare, V., Faucher, F., Breton, R. & Luu-The, V. (2005). *BMC Biochem.* **6**, 12.

Bennett, M. J., Albert, R. H., Jez, J. M., Ma, H., Penning, T. M. & Lewis, M. (1997). *Structure*, **5**, 799–812.

Collaborative Computational Project, Number 4 (1994). *Acta Cryst.* D**50**, 760–763.

Couture, J. F., Legrand, P., Cantin, L., Luu-The, V., Labrie, F. & Breton, R. (2003). *J. Mol. Biol.* **331**, 593–604.

Darmanin, C. & El-Kabbani, O. (2000). *Bioorg. Med. Chem. Lett.* **10**, 1101–1104.

Darmanin, C. & El-Kabbani, O. (2001). *Bioorg. Med. Chem. Lett.* **11**, 3133–3136.

Dhagat, U., Carbone, V., Chung, R. P.-T., Schulze-Briese, C., Endo, S., Hara, A. & El-Kabbani, O. (2007). *Acta Cryst.* F**63**, 825–830.

Dhagat, U., Endo, S., Hara, A. & El-Kabbani, O. (2008). *Bioorg. Med. Chem.* **16**, 3245–3254.

El-Kabbani, O., Ishikura, S., Wagner, A., Schulze-Briese, C. & Hara, A. (2005). *Acta Cryst.* F**61**, 688–690.

Emsley, P. & Cowtan, K. (2004). *Acta Cryst.* D**60**, 2126–2132.

Faucher, F., Cantin, L., Pereira de Jesus-Tran, K., Lemieux, M., Luu-The, V., Labrie, F. & Breton, R. (2007). *J. Mol. Biol.* **369**, 525–540.

Ishikura, S., Usami, N., Nakajima, S., Kameyama, A., Shiraishi, H., Carbone, V., El-Kabbani, O. & Hara, A. (2004). *Biol. Pharm. Bull.* **27**, 1939–1945.
Jez, J. M. & Penning, T. M. (2001). *Chem. Biol. Interact.* **130–132**, 499–525.
Jez, J. M., Bennett, M. J., Schlegel, B. P., Lewis, M. & Penning, T. M. (1997). *Biochem. J.* **326**, 625–636.
Laskowski, R. A., Moss, D. S. & Thornton, J. M. (1993). *J. Mol. Biol.* **231**, 1049–1067.
Lau, P. C. K., Layne, D. S. & Williamson, D. G. (1982*a*). *J. Biol. Chem.* **257**, 9444–9449.
Lau, P. C. K., Layne, D. S. & Williamson, D. G. (1982*b*). *J. Biol. Chem.* **257**, 9450–9456.
Matsunaga, T., Shintani, S. & Hara, A. (2006). *Drug Metab. Pharmacokinet.* **21**, 1–18.
Morris, K. D. W., Moorefield, C. N. & Amin, J. (1999). *Mol. Pharmacol.* **56**, 752–759.
Murshudov, G. N., Vagin, A. A. & Dodson, E. J. (1997). *Acta Cryst.* D**53**, 240–255.
Nahoum, V., Gangloff, A., Legrand, P., Zhu, D. W., Cantin, L., Zhorov, B. S., Luu-The, V., Labrie, F., Breton, R. & Lin, S. X. (2001). *J. Biol. Chem.* **276**, 42091–42098.
Nakagawa, M., Tsukada, F., Nakayama, T., Matsuura, K., Hara, A. & Sawada, H. (1989). *J. Biochem.* **106**, 633–638.
Oppermann, U., Filling, C., Hult, M., Shafqat, N., Wu, X., Lindh, M., Shafqat, J., Nordling, E., Kallberg, Y., Persson, B. & Jornvall, H. (2003). *Chem. Biol. Interact.* **143–144**, 247–253.
Otwinowski, Z. & Minor, W. (1997). *Methods Enzymol.* **276**, 307–326.
Penning, T. M. (2003). *Hum. Reprod. Update*, **9**, 193–205.
Penning, T. M., Burczynski, M. E., Jez, J. M., Hung, C. F., Lin, H. K., Ma, H., Moore, M., Palackal, N. & Ratnam, K. (2000). *Biochem. J.* **351**, 67–77.
Penning, T. M., Pawlowski, J. E., Schlegel, B. P., Jez, J. M., Lin, H. K., Hoog, S. S., Bennett, M. J. & Lewis, M. (1997). *Steroids*, **62**, 455–456.
Rupprecht, R. & Holsboer, F. (1999). *Trends Neurosci.* **22**, 410–416.
Storoni, L. C., McCoy, A. J. & Read, R. J. (2004). *Acta Cryst.* D**60**, 432–438.